Nuclear Materials and Energy 9 (2016) 405–410

Contents lists available at ScienceDirect

Nuclear Materials and Energy

journal homepage: www.elsevier.com/locate/nme

Behavior of W-based materials in hot helium gas

J. Matějíček[a,*], M. Vilémová[a], H. Hadraba[b], F. Di Gabriele[c], I. Kuběna[b], E. Kolíbalová[d], J. Michalička[d,e], J. Čech[f], A. Jäger[g]

[a] Institute of Plasma Physics, Za Slovankou 3, 18200 Praha, Czech Republic
[b] Institute of Physics of Materials, Žižkova 22, 61662 Brno, Czech Republic
[c] Centrum výzkumu Řež, Hlavní 130, 25068 Řež, Czech Republic
[d] Central European Institute of Technology, Technická 10, 61600 Brno, Czech Republic
[e] Tescan Orsay Holding, Libušina 1, 62300 Brno, Czech Republic
[f] Czech Technical University in Prague, Faculty of Nuclear Sciences and Physical Engineering, Trojanova 13, 12001 Praha, Czech Republic
[g] Institute of Physics, Laboratory of Nanostructures and Nanomaterials, Na Slovance 2, 18221 Praha, Czech Republic

ARTICLE INFO

Article history:
Received 10 November 2015
Revised 16 March 2016
Accepted 29 March 2016
Available online 21 April 2016

Keywords:
Tungsten
Helium
Divertor

ABSTRACT

Materials for the plasma facing components of future fusion reactors will be subjected to complex loading and various forms of interaction with low Z species (hydrogen isotopes and helium). The divertor components will be among the most intensely loaded, as they will have to transfer heat loads up to 10–20 MW/m^2. Besides the plasma facing surface being irradiated by highly energetic deuterium, tritium and helium particles from the burning plasma, the opposite surface will be exposed to a cooling medium at elevated temperature. Helium- and water-based cooling systems are currently being considered. While tungsten is the prime candidate material for the plasma facing components, in the helium-cooled divertor designs, it is also foreseen as a structural material, together with ferritic–martensitic steels. The behavior of these materials in He atmosphere at elevated temperatures has been little studied thus far, and therefore is the subject of the current work.

A number of W-based materials (pure tungsten and some of its alloys) prepared by powder metallurgy techniques was exposed to He atmosphere at 720 °C and 500 kPa for 500 h. Morphological surface changes were observed by SEM, chemical and phase composition was analyzed by EDS and XRD, respectively. The internal microstructure was observed by a combination of SEM, FIB and TEM techniques. Mechanical properties were determined by instrumented indentation. Some alloys developed a thin oxide layer, in some cases new morphological features were observed, while some samples remained mostly intact. The observed changes are correlated with specific compositions and microstructures.

Introduction

Materials for the plasma facing components of future fusion reactors will experience complex loading – thermal, mechanical, chemical etc. – and interaction with low Z species such as hydrogen isotopes and helium. For example, for the DEMO divertor components, heat loads up to ~20 MW/m^2 are foreseen [1]. The plasma facing surface will be irradiated by various particles with energies ranging from eV up to MeV (He, neutrons). As efficient active cooling will be necessary to remove the abovementioned heat loads, the opposite surface will be exposed to a cooling medium at elevated temperatures. Helium- and water-based cooling systems are currently being considered [2]. The temperature of the He coolant is expected to be in the 500–800 °C range [2–4]. While tungsten is the prime candidate material for the plasma facing components, in the helium-cooled divertor designs, it is also foreseen as a structural material, together with oxide dispersion strengthened (ODS) ferritic–martensitic steels [3–5]. The interaction of these materials with helium has been studied primarily in irradiation experiments. The effects include defect production (e.g., vacancy clusters) [6], helium embrittlement through grain boundary weakening [7], and surface changes such as the formation of pinholes [8] or He fuzz [9]. While these effects may be quite severe, they are usually limited to a thin surface layer. However, as the plasma facing components will operate at elevated temperatures, diffusion of helium from the plasma facing

* Corresponding author. Tel.: +420 266053307.
E-mail address: matejicek@ipp.cas.cz (J. Matějíček).

http://dx.doi.org/10.1016/j.nme.2016.03.009

Table 1
Overview of the samples. The last three columns present the sample weight before and after the exposure and their difference.

Number	Name	Origin	Weight before (mg)	Weight after (mg)	Difference (mg)
1	W ITER qualified	FZJ	11,659.77	11,659.45	−0.32
2	W SPS 0,7 µm, 1600 °C	IPP	8551.46	8514.34	−37.12
3	W SPS 0,7 µm, 1800 °C	IPP	6302.15	6302.08	−0.07
4	W SPS 0,7 µm 2000 °C	IPP	4369.88	4369.72	−0.16
5	W SPS 2 µm 1800 °C	IPP	7019.04	7018.99	−0.05
6	W SPS 2 µm, 2000 °C	IPP	4470.17	4470.06	−0.11
7	WCr10Ti2	CEIT	1409.16	1409.2	0.04
8	W 2%Ti	UC3M	985.55	985.66	0.11
9	W 2%V	UC3M	2191.25	2191.17	−0.08

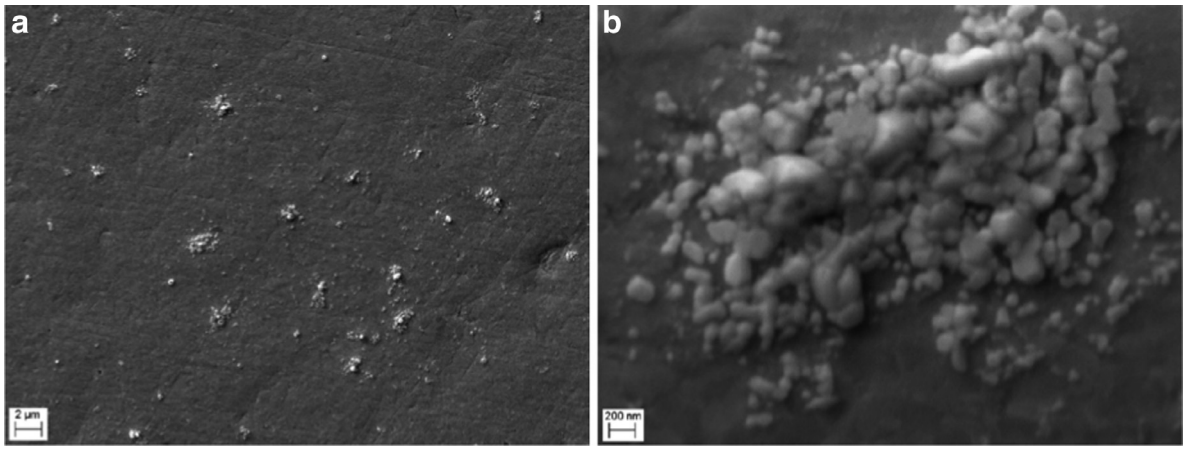

Fig. 1. Surface morphology of ITER-qualified W after exposure: (a) overview, (b) detail of a larger cluster.

surface as well as from the coolant side may induce changes in the bulk of the material. Moreover, helium may be produced within the materials as a result of tritium decay [10].

The aim of the current work is to study the behavior of bulk W-based materials in a He atmosphere at temperatures relevant for He-cooled concepts for the plasma facing components.

Experimental

Several different types of tungsten and its alloys were used in this study; their overview is provided in Table 1. Sample 1 was double-forged tungsten (99.97% purity) that meets ITER specifications [11], produced by Plansee and provided by Forschungszentrum Jülich (FZJ). Samples 2–6 were produced at the Institute of Plasma Physics, Prague (IPP) by spark plasma sintering [12] using tungsten powders (Global Tungsten & Powders, Bruntál, Czech Republic); the powder sizes and sintering temperatures are specified in Table 1. Sample 7, a self-passivating W-alloy, was produced by mechanical alloying and consolidated by hot isostatic pressing (HIP) [13] and provided by Centro de estudios e investigaciones técnicas, San Sebastián (CEIT). Such materials are intended primarily for the first wall. Samples 8 and 9 (various W-alloys) were likewise produced by mechanical alloying and HIPping [14,15] and provided by Universidad Carlos III de Madrid (UC3M).

Before the exposure, all specimens were polished the same way to 1 µm and active oxide polishing was applied as the final step. The samples were exposed to flowing helium gas (99.996% purity) at a temperature of 720 °C, pressure of 500 kPa and flow rate of 5–10 ml/min for 500 h. This is in a temperature range expected for He cooled divertors in future fusion reactors [2]. Pieces of Ti foam were also inserted in the furnace to act as a getter for oxygen impurities in the He gas.

Surface morphology changes were observed by scanning electron microscopy (SEM; Carl Zeiss SMT, Oberkochen, Germany). Changes in elemental composition were determined by energy dispersive spectroscopy (EDS) either in scanning or transmission electron microscope (TEM). Qualitative phase analysis was performed on selected samples by x-ray diffraction (XRD), using a Discover 8 (Bruker AXS, Karlsruhe, Germany) diffractometer, equipped with Cu tube, polycapillary and 2 mm collimator. Structural observations were performed by TEM on a JEM-2100F instrument (Jeol, Tokyo, Japan) with X-Max80 EDS (Oxford Instruments, Abingdon, UK) and LIBRA200FE (Carl Zeiss SMT, Oberkochen, Germany). Thin lamellae for TEM observations were prepared by a focused ion beam (FIB; Lyra 3 XMH+Canion FIB, Tescan, Brno, Czech Republic) and a precision ion polishing system (PIPS; Model 691, Gatan, Pleasanton, USA) with Ar ions accelerated at 2 kV. Sub-surface structures for SEM observations were revealed by a FIB with Ga+ source (FEI Quanta 3D FEG; FEI, Brno, Czech Republic). Basic mechanical properties (hardness and Young's modulus) were determined by instrumented indentation using a CSM NHT2 (Anton Paar, Graz, Austria) instrument with a Berkovich indenter and 500 mN load.

Results and discussion

Pure tungsten materials

Surface morphology of the ITER-qualified W after He exposure is shown in Fig. 1. While the unexposed surface was practically featureless, small scattered 'clusters' or 'nodules' appeared on the surface after the exposure. Their size ranged from ~200 nm to ~2 µm; the majority was below 1 µm. Fig. 2 shows TEM and FIB/SEM sections through such clusters. No pores, cracks or other distinct features were observed beneath these clusters. However, Fig. 2(b) shows a clear grain boundary between the cluster and the underlying grains. While only representative images are shown here, the FIB sectioning was performed on a number of these clusters, including consecutive sections on one object; the appearance

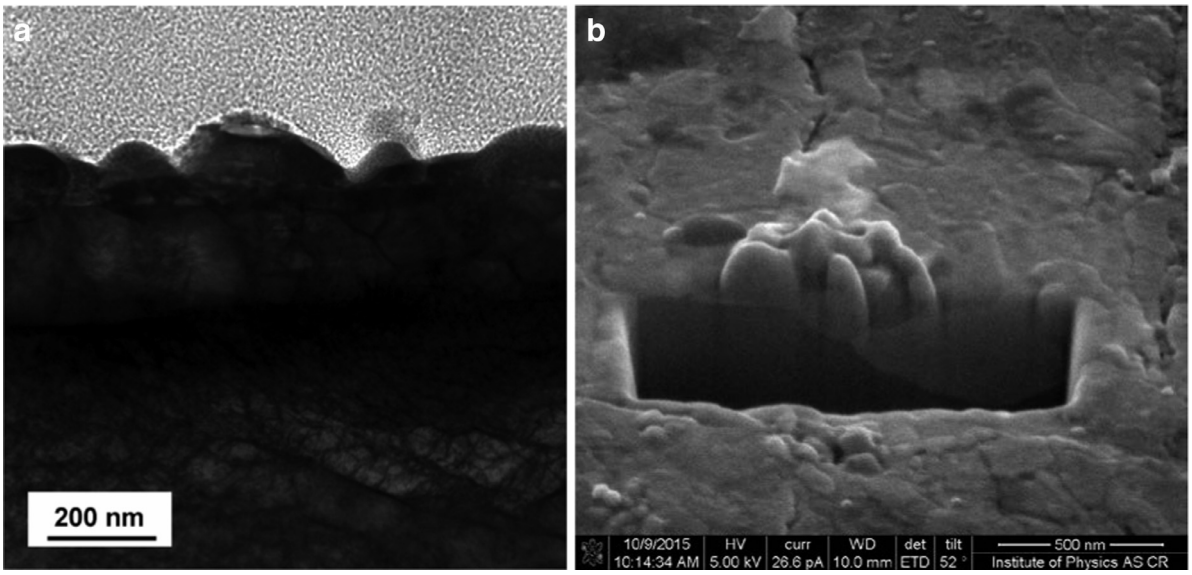

Fig. 2. (a) TEM section and (b) FIB section through representative clusters on the exposed ITER-qualified W sample.

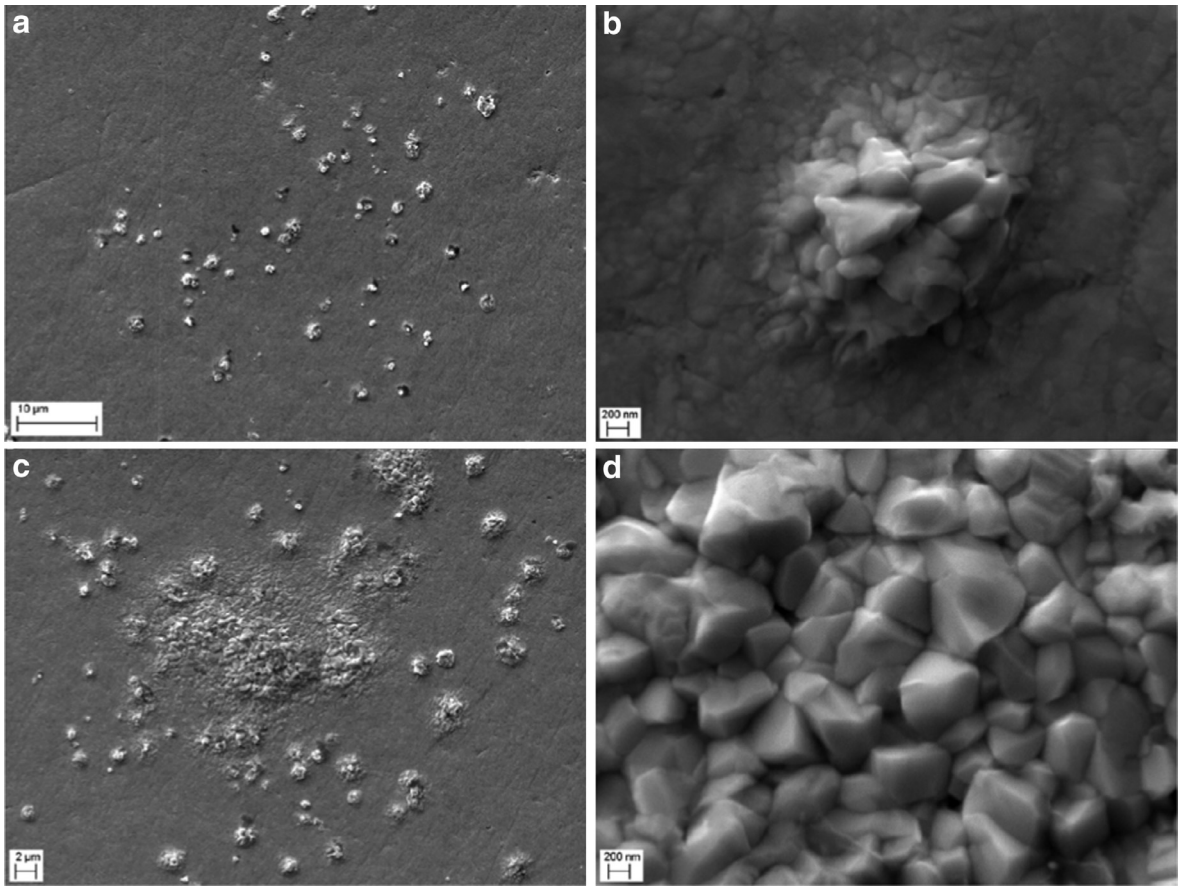

Fig. 3. Surface morphology of the exposed SPS-W (sample no. 2). (a) overview of typical small clusters, (b) detail of a small cluster, (c), (d) overview and detail of a larger cluster.

was similar in all instances. EDS on the TEM section indicated that the cluster is composed only of tungsten. While surface EDS detected some oxygen, the intensity of its signal and the size of these features were too small to unambiguously distinguish it from adsorbed oxygen on the whole surface. The mechanism of formation of these objects on tungsten surface is not clear. Perhaps some atomic-scale material transport remotely similar to He fuzz growth [16] may be responsible for this, however, the conditions are rather different.

Fig. 3 shows the surface morphology of SPS tungsten sintered at 1600 °C from 0.7 µm powder. It shows similar features as the ITER-qualified tungsten. The typical size of the clusters was around 1 µm. One exceptionally large cluster (around 10 µm) is shown in Fig. 3(c); its detail in Fig. 3(d) shows an angular, crystallite struc-

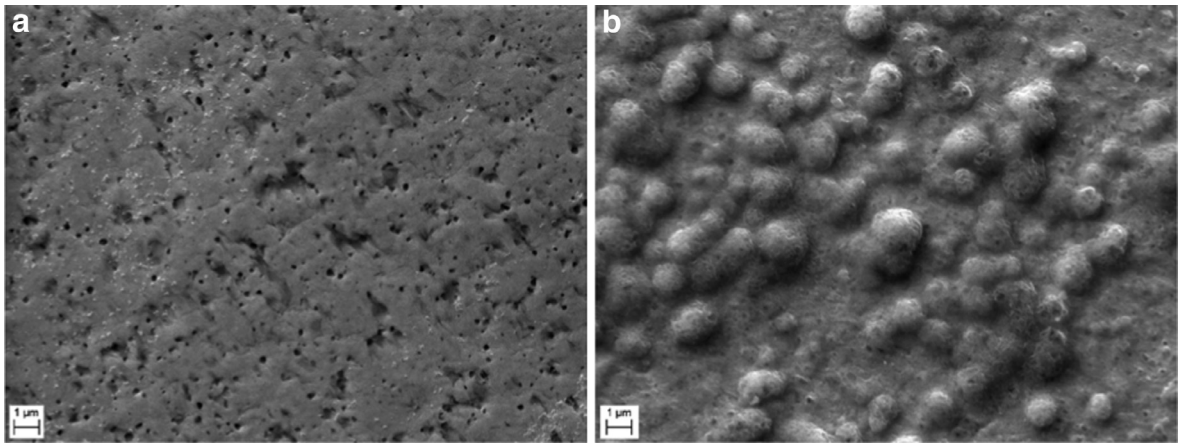

Fig. 4. Surface of the WCr10Ti2 mechanical alloy (a) before and (b) after He exposure.

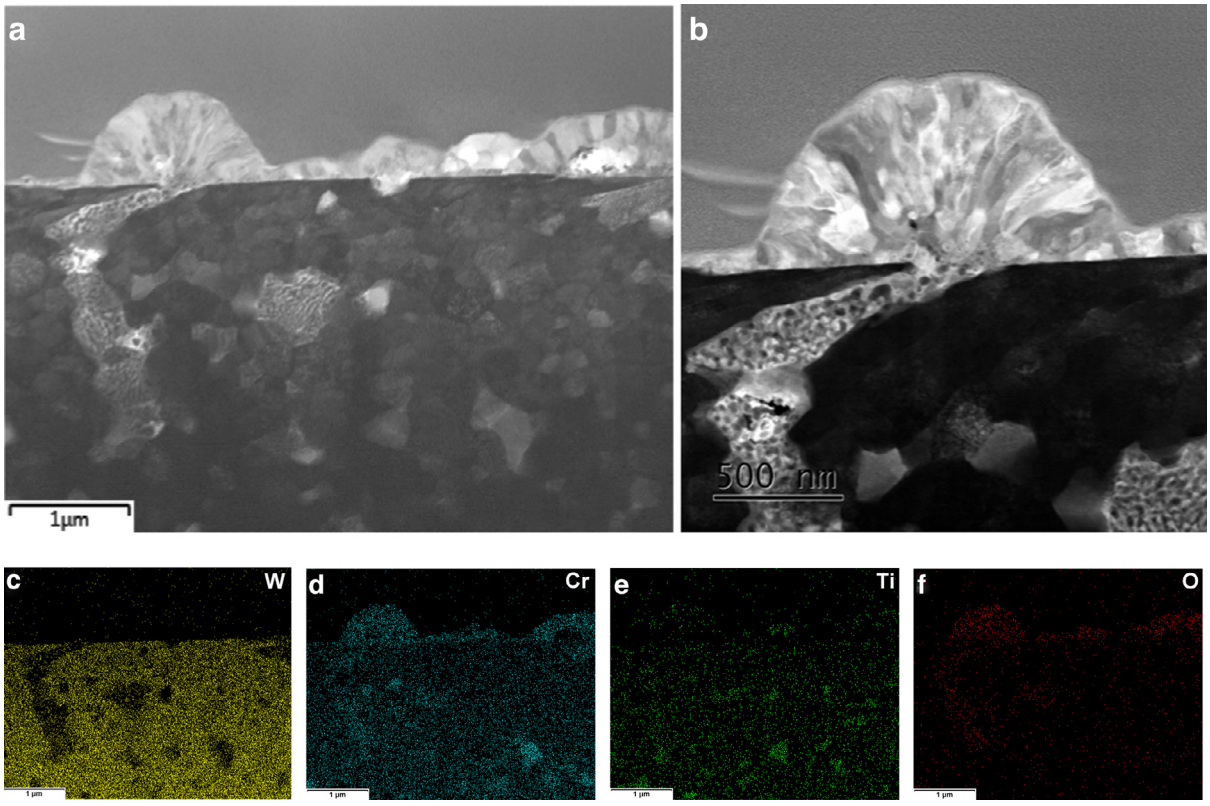

Fig. 5. (a) cross section of the surface oxide layer and subsurface structure of the exposed WCr10Ti2 sample, (b) detail of the oxide nodule, (c-f) elemental maps corresponding to the region shown in (a): (c) W, (d) Cr, (e) Ti and (f) O.

ture. On the other SPS-W samples, the clusters had a similar appearance, but their size was smaller – typically around 0.5 µm or below. The lowest typical size was observed on sample sintered from 2 µm powder at 2000 °C. Also, their occurrence was less frequent. This suggests that materials sintered at higher temperatures have higher resistance against the growth of these features. Compared to the ITER-qualified W, where the clusters were observed practically everywhere on the surface, on the SPS samples they were distributed rather randomly and sporadically.

Tungsten alloys

In the tungsten alloys, the surface morphology changes were more significant. Fig. 4 shows the surface of the WCr10Ti2 alloy before and after exposure. As can be seen in Fig. 4a (unexposed state), despite being termed 'alloy', the material still consists of a heterogeneous mixture of individual grains with varying composition (W-rich, Cr-rich, Ti-rich; see also elemental maps in Fig. 5), albeit with a very fine structure. Rietveld analysis of the XRD spectra showed about 11 wt% of the Cr-rich phase. Nevertheless, some alloying took place, as also indicated by XRD; the peaks of the major phase were shifted towards higher angles, i.e., smaller lattice constants compared to pure tungsten. Using Vegard's law, the Cr content in the W-rich phase was estimated to be 16 at%. This corresponds to 5 wt%, i.e. about half of the Cr in the initial mixture was dissolved in W and half remained in Cr-rich grains. Similarly, W content in the Cr-rich phase was estimated to be 17 at%. Due to its small amount and different crystal structure, Ti was excluded from these calculations. These results were qualitatively confirmed by EDS. Although Ti getter was used during the He exposure, some

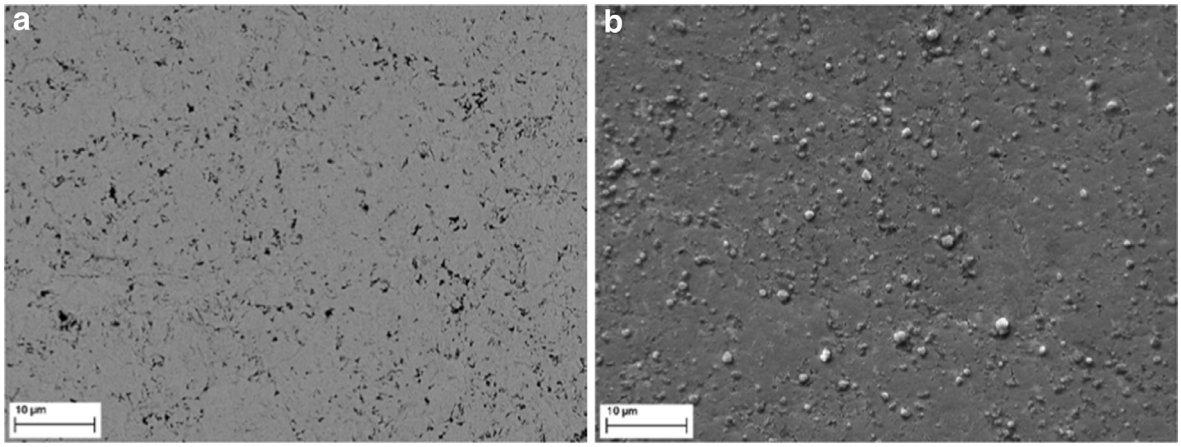

Fig. 6. Surface of the W-2Ti alloy (a) before and (b) after He exposure.

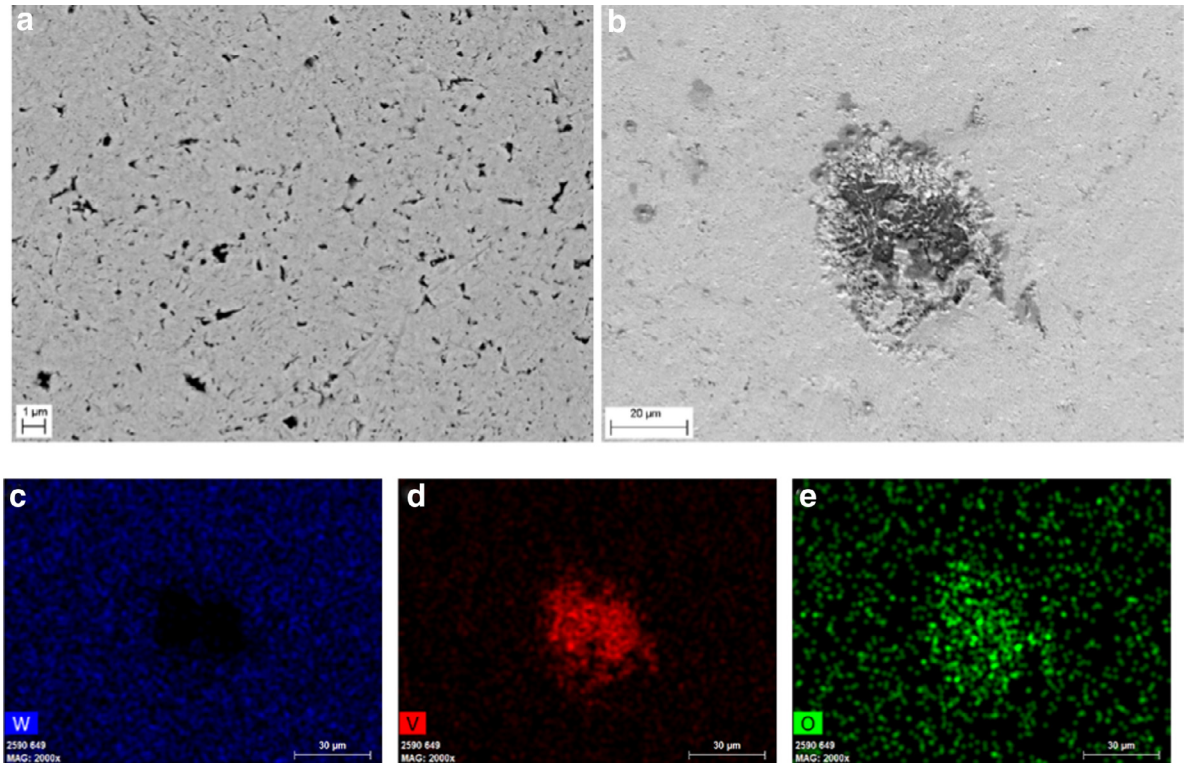

Fig. 7. Surface of the W-2V alloy (a) before and (b) after He exposure; (c–e) W, V and O elemental maps corresponding to (b).

oxidation of this alloy took place. The morphology of the oxide layer is shown in Fig. 4(b), where a contiguous oxide layer with heterogeneous thickness can be seen. XRD showed Cr_2O_3 (eskolaite) to be its dominant phase. In accordance with the preferential Cr oxidation, a slight Cr depletion in the subsurface layer, probed by x-rays, was observed. Fig. 5(a) shows a TEM section of the oxide and the subsurface region; Fig. 5(c-f) shows the corresponding elemental maps from the EDS. As can be seen, the oxide layer consists primarily of Cr and O, with some presence of Ti. The purpose of adding these elements to tungsten is to form a stable passivation layer that would prevent tungsten oxidation in the event of a loss-of-coolant accident [13]. The chromia layer grows preferentially from the Cr-rich grains, forming microscopic 'nodules', shown already in Fig. 4(b), with a detail shown in Fig. 5(b). Beneath this nodule is a 'channel' of Cr-rich oxide, penetrating deep into the bulk (left side of the image; see also Fig. 5(a) and (d)), which provides effective 'pegging' of the oxide layer in the surface. On the other hand, if the oxidation of such channels proceeds with volume increase, this may induce cracking of the W-rich matrix. Also seen in Fig. 5(b) is the radial columnar structure of this nodule, resulting from its growth starting on the outlet of the oxide channel on the surface.

Fig. 6(a) shows the structure of the W-2Ti alloy before exposure; the fine darker spots correspond to Ti-rich regions. After exposure (Fig. 6(b), numerous Ti-rich oxide nodules appeared on the surface. Their size was about 1 µm or below, i.e., slightly smaller than in the case of WCr10Ti2. In contrast to the WCr10Ti2 alloy, having formed a contiguous oxide layer as a result of higher fraction of the oxide forming elements, the oxidation of the W-2Ti alloy was limited to scattered isolated oxide nodules. The amount of the oxide was below the resolution limit of the XRD technique. The structure of the unexposed W-2V alloy also featured a dispersion of fine V-rich particles (Fig. 7(a). After exposure, small oxide nodules were observed on the surface, similarly to the W-2Ti alloy.

Table 2
Indentation hardness (H_{IT}) results.

	H_{IT} unexposed [MPa]	H_{IT} exposed [MPa]
W ITER qualified	6360 ± 160	6310 ± 150
W SPS 0.7 μm 1600 °C	5430 ± 350	5520 ± 330
WCr10Ti2	13,250 ± 310	13,400 ± 270

In a few isolated cases, larger features with rather complex morphology were observed (Fig. 7(b). EDS mapping (Fig 7(c) confirmed preferential oxidation of the V-rich regions.

As shown in Table 1, the Ti-containing alloys were the only ones that experienced weight gain, corresponding to the oxide growth. All the other samples underwent slight weight loss, which could be induced by degassing, e.g., from residual porosity. In particular, sample 2, which underwent the SPS treatment at the lowest temperature, showed the highest weight loss, which might suggest a higher sensitivity to heat treatment. Further investigations will be necessary to confirm, for example, whether the clusters appear at localized features of the grain boundaries, serving as diffusion paths for gases trapped in the material.

Mechanical properties

The results of hardness determination on selected samples are summarized in Table 2. The hardness values were largely unchanged. In the W SPS 0.7 μm 1600 °C and WCr10Ti2 samples, a slight increase was observed, however, the difference was comparable to the experimental scatter. One can note that the hardness of the WCr10Ti2 alloy is much higher than the other two materials. Young's moduli were also determined by instrumented indentation and an increase in average values was found for all three materials; however, comparable local variations were observed in some cases, therefore, no conclusions are drawn concerning the He exposure effect.

Conclusions

Several W-based materials were exposed to He gas at conditions similar to those foreseen in He-cooling divertor concepts. In pure W materials, formation of sub-micron 'clusters' on the surface was observed; these contained only tungsten. The exact formation mechanism is unknown; some small-scale material ejection due to gas pressure from inside may be speculated. Indentation did not indicate significant changes in mechanical properties due to He exposure. Therefore, one can expect only minor effects of the He exposure on the performance and survivability of W-based components. However, the pressure in this experiment was lower than that foreseen in some of the He-cooled divertor concepts (e.g. 10 MPa in [3]). A long-term exposure at higher pressures may intensify the observed effects and if the clusters detach from the base material, they may contribute to component erosion.

Materials containing the alloying elements underwent a different degree of oxidation. WCr10Ti2 formed an oxide scale covering the entire surface, with Cr_2O_3 as the dominant phase. The scale had an irregular structure with nodules and blister-like features; oxide channels also penetrated into the bulk. The W-2Ti and W-2V alloys formed only isolated oxide nodules on the surface.

In summary, pure W materials underwent minor morphological changes, with a negligible effect on mechanical properties, while Cr-, Ti- and V-containing materials experienced oxidation, preferentially of these elements. This may be expected in cooling systems with technically pure He and may be more severe during long-term operation. The oxidation may be suppressed by using high purity helium.

Acknowledgments

This research was supported by the following: Czech Science Foundation (grant nos. 14-12837S and 14-25246S), Czech Academy of Sciences (Strategy AV21), European Regional Development Fund (CZ.1.05/2.1.00/03.0108), Ministry of Education, Youth and Sports of the Czech Republic (LM2011020 and LM2011026), Ministry of Industry and Trade (4.2 PT03/586). Thanks are also due to Ángel Muñoz (UC3M), Carmen García-Rosales (CEIT) and Marius Wirtz (FZJ) for kindly providing W samples.

References

[1] D. Stork, P. Agostini, J.L. Boutard, D. Buckthorpe, E. Diegele, S.L. Dudarev, C. English, G. Federici, M.R. Gilbert, S. Gonzalez, A. Ibarra, C.H. Linsmeier, A. Li Puma, G. Marbach, P.F. Morris, L.W. Packer, B. Raj, M. Rieth, M.Q. Tran, D.J. Ward, S.J. Zinkle, J. Nucl. Mater. 455 (2014) 277–291.
[2] D. Stork, DEMO and the Route to Fusion Power (2009).
[3] P. Norajitra, S. Antusch, L.V. Boccaccini, M. Kuzmic, I. Maione, L. Spatafora, Fusion Eng. Des. 87 (2012) 932–934.
[4] J. Reiser, M. Rieth, Fusion Eng. Des. 87 (2012) 718–721.
[5] J. Aktaa, W.W. Basuki, T. Weber, P. Norajitra, W. Krauss, J. Konys, Fusion Eng. Des. 89 (2014) 913–920.
[6] A. De Backer, C.J. Ortiz, C. Domain, M.F. Barthe, C.S. Becquart, Nucl. Instrum. Methods B 303 (2013) 87–90.
[7] V.I. Gerasimenko, I.M. Mikhailovskii, I.M. Neklyudov, A.A. Parkhomenko, O.A. Velikodnaya, Tech. Phys. 43 (1998) 803–808.
[8] X. Shu, B.O. Huang, J. Yang, D. Liu, H. Fan, J. Liao, Y. Yang, N. Liu, J.U.N. Tang, Fusion Sci. Technol. 66 (2014) 278–282.
[9] G. De Temmerman, T.W. Morgan, G.G. Van Eden, T. De Kruif, M. Wirtz, J. Matejicek, T. Chraska, R.A. Pitts, G.M. Wright, J. Nucl. Mater. 463 (2015) 198–201.
[10] M.I. Baskes, MRS Bull. 11 (1986) 14–18.
[11] T. Hirai, F. Escourbiac, V. Barabash, A. Durocher, A. Fedosov, L. Ferrand, T. Jokinen, V. Komarov, M. Merola, S. Carpentier-Chouchana, N. Arkhipov, V. Kuznetcov, A. Volodin, S. Suzuki, K. Ezato, Y. Seki, B. Riccardi, M. Bednarek, P. Gavila, J. Nucl. Mater. 463 (2015) 1248–1251.
[12] B. Nevrlá, M. Vilémová, J. Matějíček, in: Proceedings of the XIIIth Youth Symposium on Experimental Solid Mechanics, Czech Technical University in Prague, 2014, pp. 80–83.
[13] P. Lopez-Ruiz, N. Ordas, I. Iturriza, M. Walter, E. Gaganidze, S. Lindig, F. Koch, C. Garcia-Rosales, J. Nucl. Mater 442 (2013) S219–S224.
[14] J. Martinez, B. Savoini, M.A. Monge, A. Munoz, D.E.J. Armstrong, R. Pareja, Fusion Eng. Des. 88 (2013) 2636–2640.
[15] A. Munoz, B. Savoini, E. Tejado, M.A. Monge, J.Y. Pastor, R. Pareja, J. Nucl. Mater. 455 (2014) 306–310.
[16] S. Kajita, W. Sakaguchi, N. Ohno, N. Yoshida, T. Saeki, Nucl. Fusion 49 (2009) 095005.